Attaining Inhibition of Sneak Current and Versatile Logic Operations in a Singular Halide Perovskite Memristive Device through Introducing Appropriate Interface Barriers

Song He, [a] Xingyu Yu, [a] Juanjuan Wang, [a] WenKang Zhong, [a] Baochang Cheng [a, b] and Jie Zhao *[a]

[a] *School of Physics Materials, Nanchang University, Jiangxi 330031, P. R. China*

[b] *Nanoscale Science and Technology Laboratory, Institute for Advanced Study, Nanchang University, Jiangxi 330031, P. R. China*

**Correspondence to: E-mail: ncu915@outlook.com*

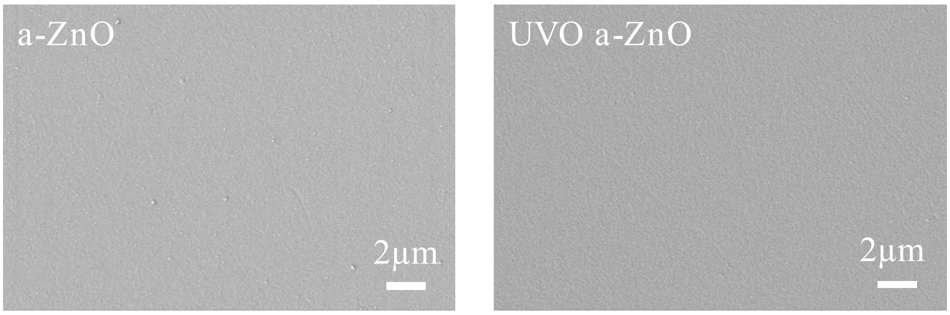

Fig. S1 Top-view SEM images of UVO-treated and untreated a-ZnO films

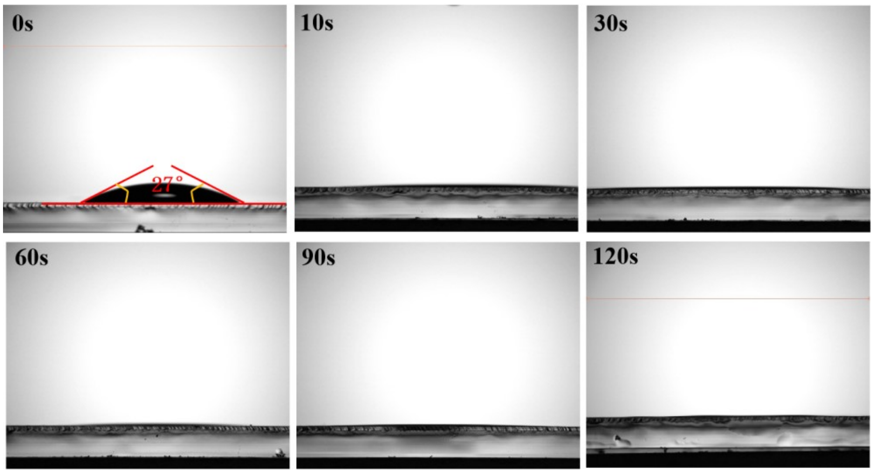

Fig. S2 DMSO: DMF solution contact angle on a-ZnO films with verious UVO-treated time

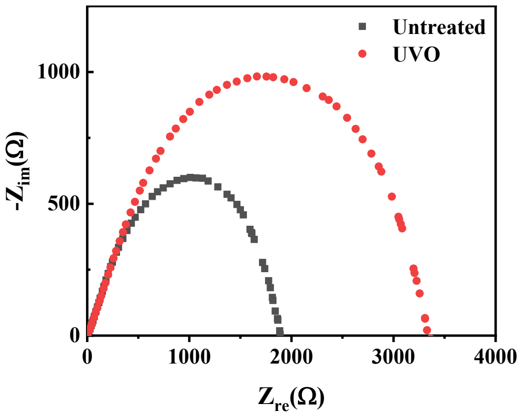

Fig. S3 The IS spectra evolution of the untreated device and the UVO-treated device.

Electrochemical impedance spectroscopy was conducted to provide further insights. The Nyquist diagram, as depicted in the figure, was obtained, and the device in this study was fitted to an equivalent circuit. In the low-frequency region, the carrier recombination resistance (Rrec) becomes evident, forming a semicircle. The Rrec values for the untreated device and the device after 120 seconds of UV ozone treatment were 1890 Ω and 3328Ω, respectively. It is apparent that the composite impedance of the UV ozone-treated device is higher than that of the untreated device, indicating successful UVO treatment. This treatment enhances carrier recombination, aids in improving charge extraction and transport, and reduces interface charge accumulation within the device.

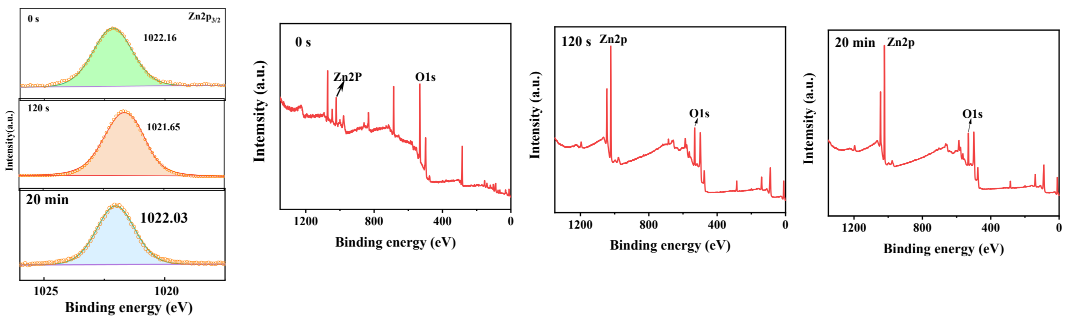

Fig. S4 High-resolution Zn $2p_{3/2}$ XPS core level spectrum and the full spectrum

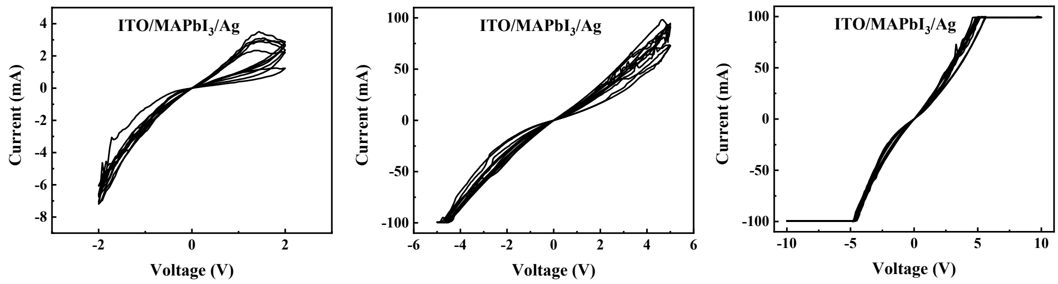

Fig. S5 I-V characteristics of ITO/ $MAPbI_3$/Ag tested by different amplitude of voltages.

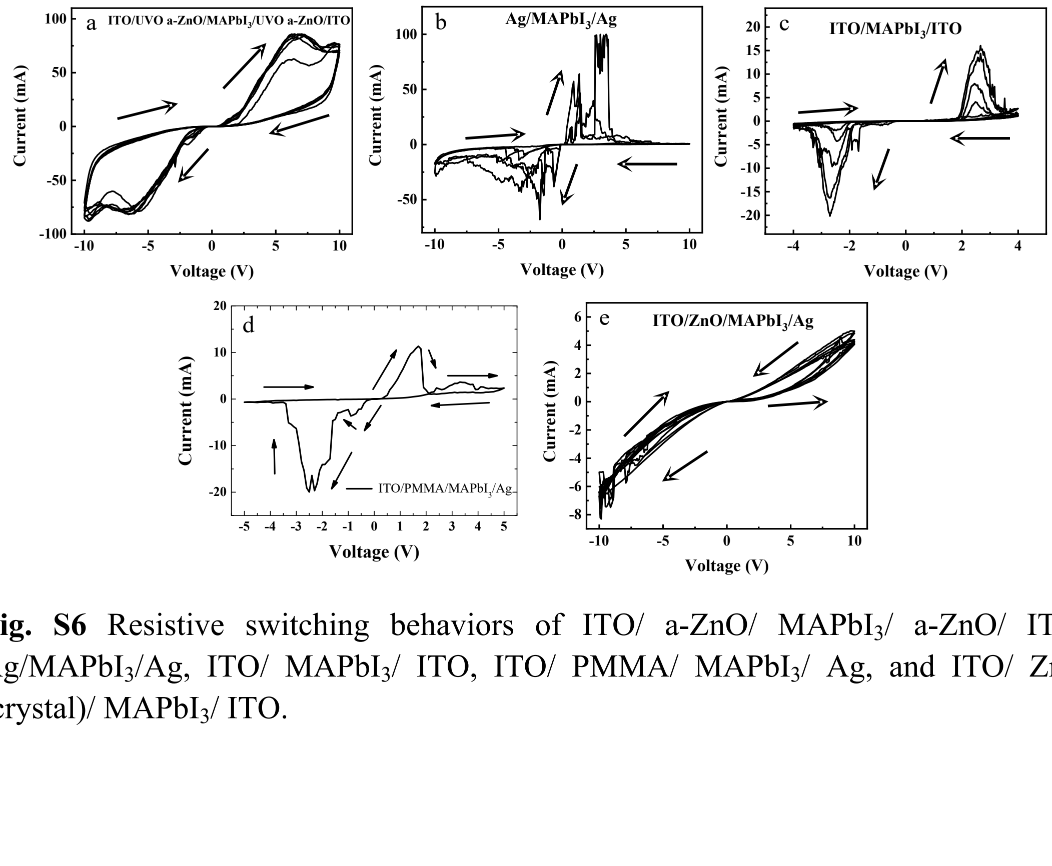

Fig. S6 Resistive switching behaviors of ITO/ a-ZnO/ $MAPbI_3$/ a-ZnO/ ITO, Ag/$MAPbI_3$/Ag, ITO/ $MAPbI_3$/ ITO, ITO/ PMMA/ $MAPbI_3$/ Ag, and ITO/ ZnO (crystal)/ $MAPbI_3$/ ITO.

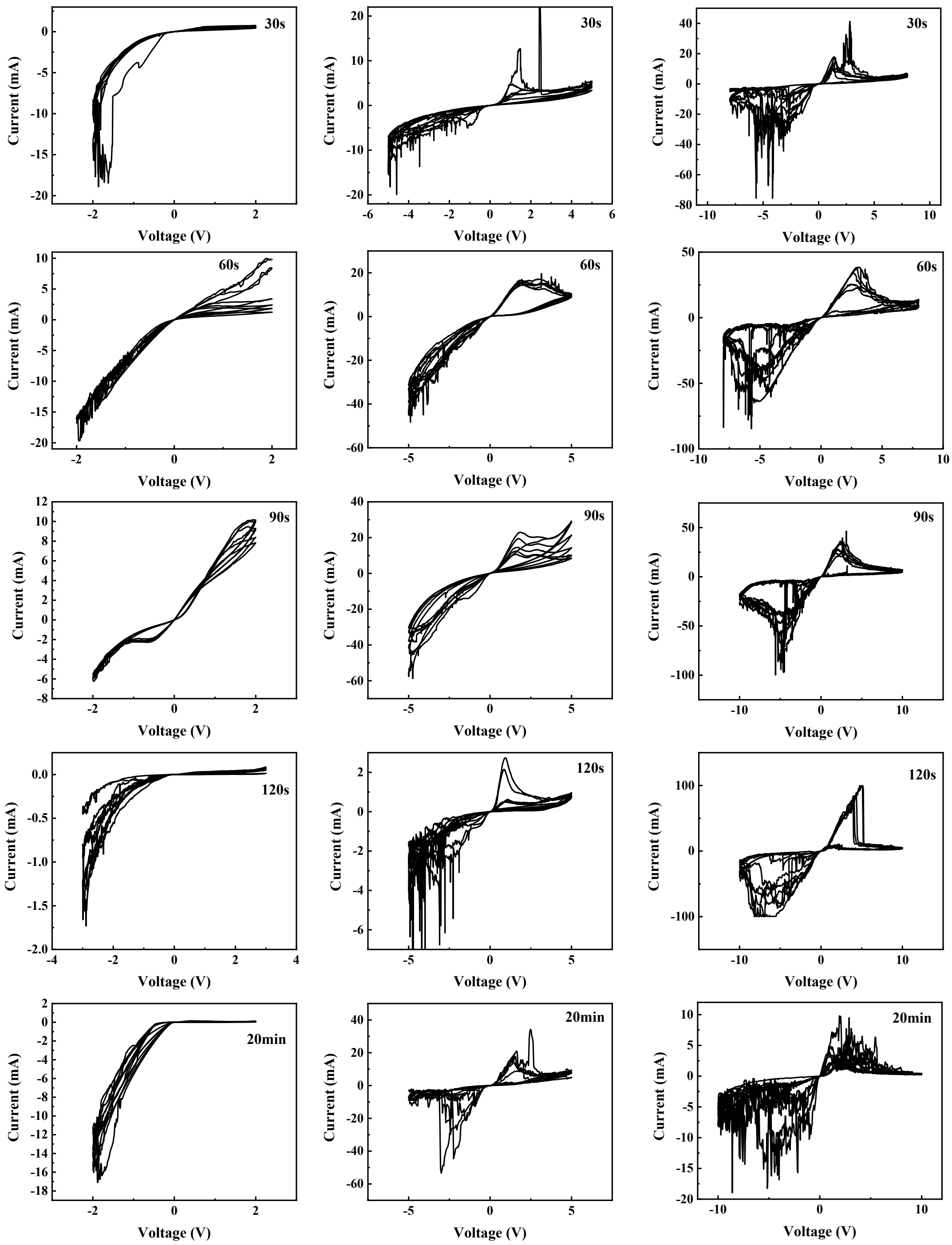

Fig. S7 A series of RS behaviors of UVO-treated devices under various voltage amplitudes and different treatment times.

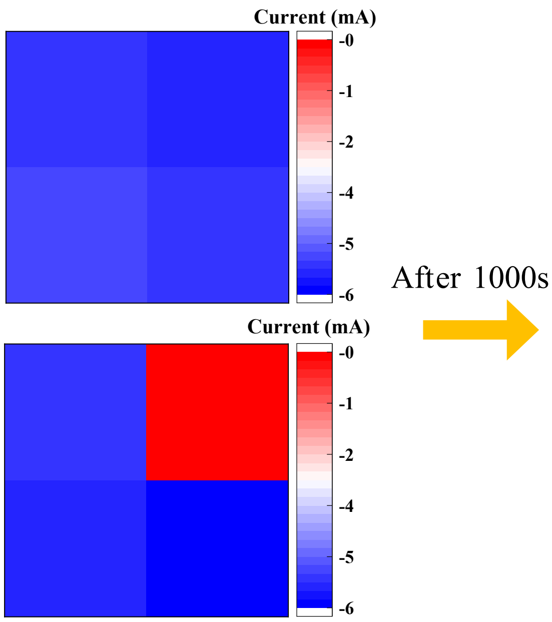

Fig. S8 The currents within a 2×2 cross array were observed over a 1000 s duration, showcasing the endurance of the maintained resistance state in OHP RRAMs.

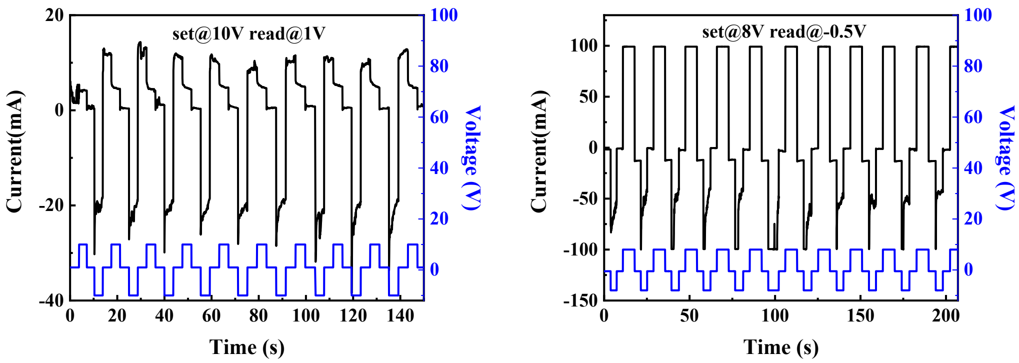

Fig. S9 Multiple writing-erasing processes of the nonvolatile OHP RRAMs.

Tab. S1 Comparison of various halide perovskites -based ReRAM devices.

Structure	**RS type**	**SET (V)**	**RESET (V)**	**Stable Endurance (times)**	**Retention (s)**	**ON/OFF Ratio**	**Ref.**
Au/$CH_3NH_3PbI_{3-x}Cl_x$/FTO	bipolar	0.8	-0.6	10^2	10^4	2	1
FTO/TiO_2/$MAPbI_3$/Spiro-MeOTAD/Ag	bipolar	+0.8	-0.8	2×10^2	2.4×10^4	6	2
PET/multilayer graphene/$MAPbI_3$/Au	bipolar	+0.68	-0.5	5×10^2	10^4	30	3
FTO/$MAPbI_3$/AgInSbTe/Ag	bipolar	+0.5	-0.3,0.6	1.2×10^2	10^4	20	4
FTO/$MAPbI_3$/Al	bipolar	+1.5	-1.4	10^3	/	20	5
FTO/$MAPbI_3$/Au	bipolar	+1	-1	1×10^2	10^4	40	6
FTO/$MAPbI_3$/W	bipolar	+3.1	-1.1	1×10^2	/	200	7
ITO/PEDOT:PSS/perovskite/Bphen(20 nm)/Ag	bipolar	2.1	6	6×10^1	/	64	8
ITO/$CH_3NH_3PbI_3$/Ag	bipolar	+0.32	-0.42	5×10^2	10^3	1000	9
ITO/$MAPbBr_3$/$MAPbBr_3$/ITO	Unipolar	7.5	/	6×10^2	4×10^1	80	8
ITO/$MAPbBr_3$/Au	threshold switch	+1	-1	10^3	10^4	10^3	10
ITO/$MAPbI_3$/Au	Symmetrical NDR	1	/	10^2	10^4	50	6
Ag/$MAPbI_3$/Ag	Symmetrical NDR	±0.1	±0.4	7.5×10^1	7.5×10^2	7.5	11
Ag/$MAPbI_3$/C	Symmetrical NDR	/	/	/	/	2 (light)	12
Ag/$MAPbI_3$/Ag	Symmetrical NDR	-5	5	/	/	4 (light)	13
ITO/UVO a-ZnO/$MAPbI_3$/Ag	Symmetrical NDR	±5	±6	5×10^2	2×10^3	80	This work

References:

1. E. J. Yoo, M. Lyu, J. H. Yun, C. J. Kang, Y. J. Choi and L. Wang, Advanced Materials, 2015, 27, 6170-6175.
2. G. Landi, V. Subbiah, K. S. Reddy, A. Sorrentino, A. Sambandam, P. C. Ramamurthy and H.-C. Neitzert, IEEE Journal of the Electron Devices Society, 2018, 6, 454-463.
3. C. W. Jang, S. W. Hwang, S. H. Shin and S.-H. Choi, Journal of the Korean Physical Society, 2018, 73, 934-939.
4. W. Wang, J. Xu, H. Ma, X. Zhao, Y. Lin, C. Zhang, Z. Wang, H. Xu and Y. Liu, ACS Applied Nano Materials, 2018, 2, 307-314.
5. Y. Ren, H. Ma, W. Wang, Z. Wang, H. Xu, X. Zhao, W. Liu, J. Ma and Y. Liu, Advanced Materials

Technologies, 2019, 4, 1800238.
6. H. Ma, W. Wang, H. Xu, Z. Wang, Y. Tao, P. Chen, W. Liu, X. Zhang, J. Ma and Y. Liu, ACS applied materials & interfaces, 2018, 10, 21755-21763.
7. H. Cai, G. Ma, Y. He, C. Liu and H. Wang, Organic Electronics, 2018, 58, 301-305.
8. X. Yu, T. Shen, C. Zhu, Q. Zeng, A. Yu, S. Liu, R. Yi, Z. Weng, Y. Zhan and X. Hou, ACS Applied Nano Materials, 2020, 3, 11889-11896.
9. S. Ham, S. Choi, H. Cho, S. I. Na and G. Wang, Advanced Functional Materials, 2019, 29, 1806646.
10. X. Guan, W. Hu, M. A. Haque, N. Wei, Z. Liu, A. Chen and T. Wu, Advanced Functional Materials, 2018, 28, 1704665.
11. J. Zhao, S. Li, W. Tong, G. Chen, Y. Xiao, S. Lei and B. Cheng, Advanced Electronic Materials, 2018, 4, 1800206.
12. R. Gou, Z. Ouyang, C. Xu, S. He, S. Cheng, C. Shi, J. Zhao, Y. Xiao, S. Lei and B. Cheng, Nanoscale Horizons, 2022, 7, 1095-1108.
13. R. Gou, C. Xu, Z. Ouyang, S. He, Y. Xiao, S. Lei, B. Cheng and J. Zhao, Journal of Alloys and Compounds, 2023, 968, 172042.